Adsorptive removal of synthetic food dyes using low-cost biochar: Efficiency prediction, kinetics and desorption index evaluation

Deborah Temitope Bankole [a,b,*], Adejumoke Abosede Inyinbor [a,b,*], Abimbola Peter Oluyori [a], Micheal Olaolu Arowolo [c]

[a] Department of Physical Sciences, Landmark University, P.M.B 1001, Omu Aran, Nigeria
[b] Clean Water and Sanitation Sustainable Development Goal, Landmark University, P.M.B 1001, Omu Aran, Nigeria
[c] Department of Electrical Engineering and Computer Science, University of Missouri, Columbia, USA

ARTICLE INFO

ABSTRACT

Low-cost biochar prepared from *Bilghia sapida* wastes (BSAB) was utilized in the adsorption of Allura red (ARFD) and Sunset Yellow (SYFD) food dyes. The activation process increased the BET surface area from 970.25 to 1122.05 m^2/g. The maximum adsorption capacities were obtained as 15.17 and 33.27 mg/g for ARFD and SYFD respectively. The kinetic model's analysis indicated that both internal and surface diffusion occurred in the adsorption systems. The desorption investigations revealed that all of the desorbing agents had low efficiency. This was substantiated by the desorption index values (1.0188 and 1.3831) for ARFD and SYFD, indicating low degree of reversibility. As predicted by the ANN model, the best transfer function, MSE and R^2 values were (*Logsig*, 9.96, 0.9771) for ARFD and (*Tansig*, 10.88, 0.9835) for SYFD. Consequently, BSAB have a considerable potential for the adsorption of food dyes from confectionary industrial wastewaters.

1. Introduction

Toxic industrial wastes are byproducts of industrial revolution, causing major environmental degradation and health hazards. Researchers continue to work to eradicate issues caused by industrial waste toxins emanating from diverse industries. Food and confectionary industry is one of such industries. Food dyes such as Allura red (ARFD) and Sunset Yellow (SYFD) are azo-based colours used to improve the quality or create an appealing look in foods. It should be emphasized that several of these colours pose major health hazards (Hosseinian-Roudsari et al., 2022; Šuleková et al., 2017). Many azo dyes are carcinogenic and mutagenic in nature and are capable of triggering allergic responses (Gičević et al., 2020). Also, many countries tend to boost their economic development by tackling wastewaters from these industries, which is frequently underestimated (Moradi and Sharma, 2021). Several techniques, including membrane separation, photodegradation, bioremediation, ultrafiltration and adsorption among others, have been used to eradicate dyes from wastewater (da Silva Alves et al., 2021; Fu et al., 2021; Oladipo et al., 2021). The adsorption method is the most basic and cost-effective of these techniques.

Adsorption is a pre-treatment phase in the water purification industry which offers features such as simplicity, minimal sludge generation, significant reuse capability, easy and handy operation (Inyinbor et al., 2023b; Obayomi et al., 2023). Commercial activated carbon, which is frequently used in adsorption operations is expensive. As a result, proper utilization of agricultural biomass yields significant economic and social benefits (Obayomi et al., 2023; Tokula et al., 2023). Biochar is a product obtained from the pyrolysis of various biomasses such as agricultural, industrial and municipal solid wastes. Biochar is gaining acceptance due to its high carbon content, excellent adsorption ability, large specific surface area and stable structure. Biochar preparation does not only eliminate wastes but also embodies the concept of resource reuse (Bashir et al., 2022; Inyinbor et al., 2023b).
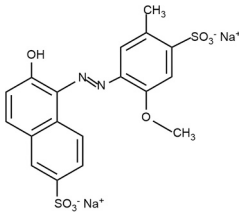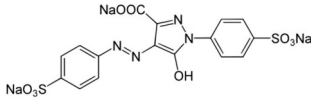
Artificial Neural Networks (ANN) are useful tools for modelling complex functional relationships like adsorption processes (Ghaedi et al., 2015). ANN offers advantages such as accurate correlation, simplicity, adaptability and prediction skills for addressing multivariable problems with non-linear behaviour. These features have justified its use in the investigation and simulation of adsorption processes (Reynel-Ávila et al., 2022).

The utilization of acid-activated *Bilghia sapida* seed pods (BSAB) as a workable adsorbent for food dyes (ARFD and SYFD) has not been

---

Table 1
Properties of Allura red and Sunset yellow food dyes.

Properties		
Common name	Allura red	Sunset yellow
Generic name	FD&C Red 40	FD&C Yellow
CAS number	25,956–17-6	2783-94-0
Colour index number	16,035	15,985
Colour	Dark red	Orange red
Maximum wavelength (nm)	505	480
Molecular weight (g/mol)	496.4	432.4
Empirical formula	$C_{18}H_{14}N_2Na_2O_8S_2$	$C_{16}H_{13}N_2NaO_7S_2$
Chemical structure		

documented in the literature, hence this study explores a novel approach. In this study, the isothermal and kinetic studies as well as the impact of various adsorption variables on ARFD and SYFD uptake onto BSAB were explored. The desorption studies and desorption index were investigated to ascertain the reusability potential of BSAB. The ANN model in the MATLAB R2016a software was employed to forecast the adsorption efficiencies at various temperatures. Furthermore, the cost analysis was implemented to establish the practicability of commercializing BSAB.

2. Materials and methods

2.1. Chemicals and food dyes

The pure sunset yellow dye ($C_{16}H_{10}N_2Na_2O_7S_2$, 480 nm) was purchased for Loba Chemie PVT Ltd. while the allura red dye ($C_{18}H_{14}N_2Na_2O_8$, 505 nm) was acquired from Central Grug House Ltd. Vardaam House, New Delhi India. The properties of Allura red and Sunset yellow food dyes is presented in Table 1. The orthophosphoric acid, hydrochloric acid (HCl), sodium hydroxide (NaOH), sodium chloride (NaCl) and all other reagents were of analytical grade.

2.2. Sample collection, preparation, carbonization and characterization

Temitope Bankole et al., 2022 previously reported the full methodology involved the collection, preparation and activation of BSAB (Temitope Bankole et al., 2022). The functional groups present on the surface of BSAB were investigated using the Fourier Transformed Infrared (FTIR) model: (Thermo Nicolet iS10, USA) in the 4000 cm^{-1} to 400 cm^{-1}. Prior to analysis, the material was degassed for 6 h. A micrometric porosity (Micrometrics Tri-star II, USA) and surface area analyser was used to estimate the Brunauer-Emmett-Teller (BET) specific surface area, size, and pore volume. The surface structure of the generated biochar was identified using scanning electron microscopy (JEOL JSM-7600F, Japan). EDX was used to study the elemental composition; the line spectra obtained correspond to each of the elements present, and the strength of the peak lines equates to the concentration of each component (element).

2.3. Adsorption and desorption experiments

A mechanical shaker (SHA-C water bath shaker, China) with a thermostat was used to conduct the batch experiment. Adsorption agitation is accomplished by varying the shaker's vibration at a rate of 120 rotations per minute. To keep the temperature constant at the desired level, the thermostatic knob was adjusted. Erlenmeyer conical flasks with a capacity of 250 mL were used for the adsorption process. Varying pH (2−10), times, doses (0.05–0.25 g/100 mL), initial ARFD and SYFD concentrations (5–20 mg/L), and temperatures (26–55 °C) are taken into consideration for the batch setup. By adding 0.1 M HCl and 0.1 M NaOH, the pH of the solution was adjusted. The amount of adsorbent utilized for the entire experiment was 0.01 g/100 mL of dye solution. The supernatant solution was then analysed in a UV-spectrophotometer (Biochrome Libra 160 UV–visible spectrophotometer) at the end of each experiment. The remaining dye content was calculated using the calibration curves for ARFD and SYFD respectively. Eqs. (1a) and (1b) was used to compute the quantity of dye adsorbed and % dye removal respectively. The desorption experiments were conducted with four different eluents: 20 mL of 0.1 M HCl, 0.1 M NaOH, deionized water, and 0.1 M NaCl. Eqs. (2a) and (2b) was employed to calculate the percentage of dye desorbed. The desorption index, which can also be calculated using Eq. (3), aids in determining the degree of reversibility of an adsorption process. All experiments were carried out in duplicates and the data presented as mean ± Standard deviation.

$$q_t = \frac{(C_o - C_t)V}{W} \tag{1a}$$

$$\%Re = \left\{ \frac{C_o - C_e}{C_o} \right\} \times 100 \tag{1b}$$

$$q_{des} = C_{des}\frac{V}{W} \tag{2a}$$

$$\%Desorption\ Efficiency = \frac{q_{des}}{q_e} \times 100 \tag{2b}$$

$$Desorption\ index = \frac{\%dye\ remove\ after\ adsorption}{\%dye\ removed\ after\ desorption} \tag{3}$$

2.4. Artificial Neural Network prediction

The ANN topography is made up of layers, the number of neurons that serve as processing units in each layer and transfer functions. This segment attempted to create an ANN model that could accurately predict the effectiveness of BSAB for ARFD and SYFD adsorption. The ANN model was constructed using the mathematical software MATLAB 2016a. The datasets generated during the experimental technique were used to construct the model architecture. These data were generated from the effects of operational parameters such as adsorbate pH, ARFD and SYFD initial concentrations, contact time, temperature, and BSAB dosage and the corresponding adsorption efficiencies. These operational parameters also made up the composition of the input variables while

Table 2
Properties of the prepared biochar.

Property	BSAB
pH_{pzc}	3.00 ± 0.02
BET surface area (m^2/g)	1122.05
Langmuir surface area (m^2/g)	980.05
Bulk density (g/cm^3)	0.375
Pore volume (cm^3/g)	0.6065
Pore size (Å)	30.55
% Fixed carbon	65.70
EDS % carbon	80.43
% Moisture	4.59
% Ash content	11.08

the target/output was the % adsorption efficiency calculated from the input variables. For ARFD uptake, a total of 1309 data sets were splitted into (916, 197, and 197) for training (70 %), validation (15 %), and testing (15 %). Whereas for SYFD, 1518 datasets were divided into 1062, 288 and 288 datasets. By varying the hidden neurons between 1 and 20, the Levenberg-Marquardt algorithm was employed to evaluate the optimal fit. For further training using different activation functions, the hidden neuron with the lowest mean square error was selected. The adsorption efficiency was then predicted using the network with the most suitable parameters, and the ANN model architecture was developed.

3. Results and discussion

3.1. Biochar characterization

3.1.1. Physicochemical properties

The physiochemical properties of biochar vary depending on the type of precursor and the process of Pyrolysis carbonization used to prepare the biochar (Wang and Wang, 2019). The properties of BSAB is presented in Table 2. BSAB has a relatively high BET surface area of 1124.25 m^2/g, pore size of 30.55 Å and pore volume of 0.6065 cm^3/g, which could be attributed to the impact of the chemical activation. The pore diameter classifies the adsorbent as mesoporous according to IUPAC classification (Ahmad et al., 2016).

3.1.2. Fourier Transformed Infrared analysis

Before adsorption, the FTIR analysis of BSAB revealed multiple distinct peaks as shown in Fig. S1. The FTIR spectrum of BSAB exhibited a more intense band at 3420 cm^{-1}, an attribute of −OH functional group vibration, which could be owed to an increase in hydroxyl groups after the biomass was exposed to orthophosphoric acid activating agent. The symmetric −CH stretching within the BSAC structure is reflected by the distinctive peaks at 2921 cm^{-1}. The vibrational stretching of C=O is represented by the sharp transmittance band at 1610 cm^{-1}. The bands at 1230 cm^{-1} is assigned to C−N stretching of aromatic amines whereas the peak designated at 1080 cm^{-1} is an attribute of C−O stretching vibration. Evidence of participation of certain functional groups in the adsorption process is an emergence of new peaks, while some peaks have vanished or shifted. Notably, the appearance of sharp peaks at 2930 and 1030 cm^{-1} for ARFD adsorption. Similar findings have been documented (Al Shamari et al., 2020; Reyna G et al., 2023; Saha et al., 2020).

3.1.3. Scanning electron microscopy analysis

The surface of the extremely porous and irregularly structured BSAB was entirely occupied after the uptake of ARFD and SYFD molecules, as seen in SEM micrographs taken before (Fig. S2a) and after the uptake of ARFD (Fig. S2b) and SYFD molecules (Fig. S2c). This process considerably altered the surface of BSAB which is as a result of successful adsorption process (Darryle et al., 2021).

3.2. Effects of operational variables

3.2.1. Influence of pH

Depending on the pH of the aqueous solution, the functional groups on SYFD, ARFD and BSAB can be deprotonated or protonated. This results in the electrostatic attraction or repulsion of the charged adsorbates and adsorbents (Saha et al., 2020). The quantities of ARFD and SYFD adsorbed onto BSAB at different pH, was estimated by varying the pH of the solution between 2 and 10. The effect of pH for ARFD and SYFD uptake onto BSAB is depicted in Fig. 1. For ARFD, the maximum adsorption efficiency of 91.04 % was obtained at pH of 4. At pH of 4, ALR is highly protonated, while BSP1 is anionic (pH > pHpzc (3)). Hence the optimum adsorption at pH 4. Generally, relatively high removal efficiencies were obtained between. This can be due to the fact that, ARFD is an anionic dye molecule, with sulfonate groups, which can be electrostatically attracted to the cationic surface of BSAB (Saloglu and Irmak, 2021).

In the case of SYFD, removal efficiencies obtained between 83.64 and 86.34 % in the pH range of 4 and 7 could be explained as follows. SYFD
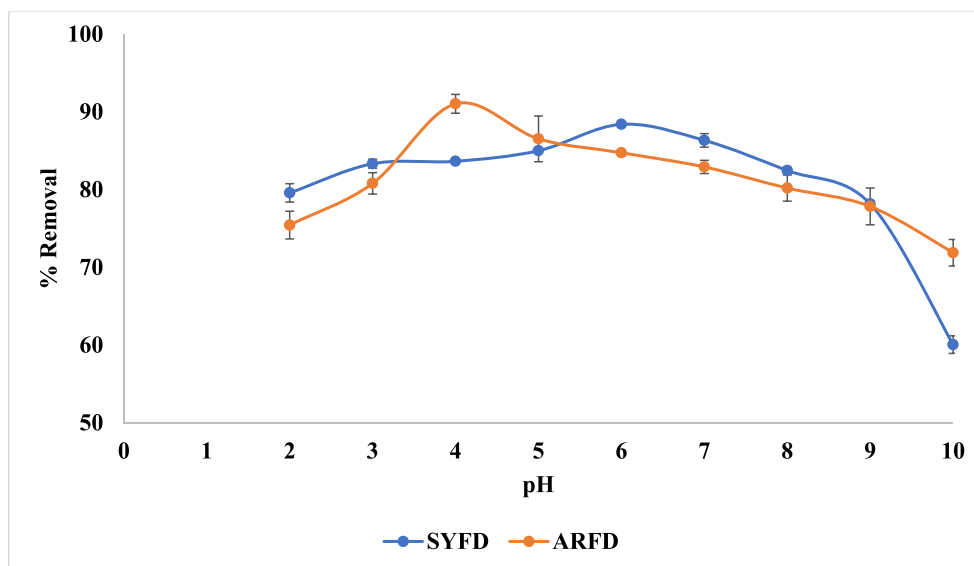

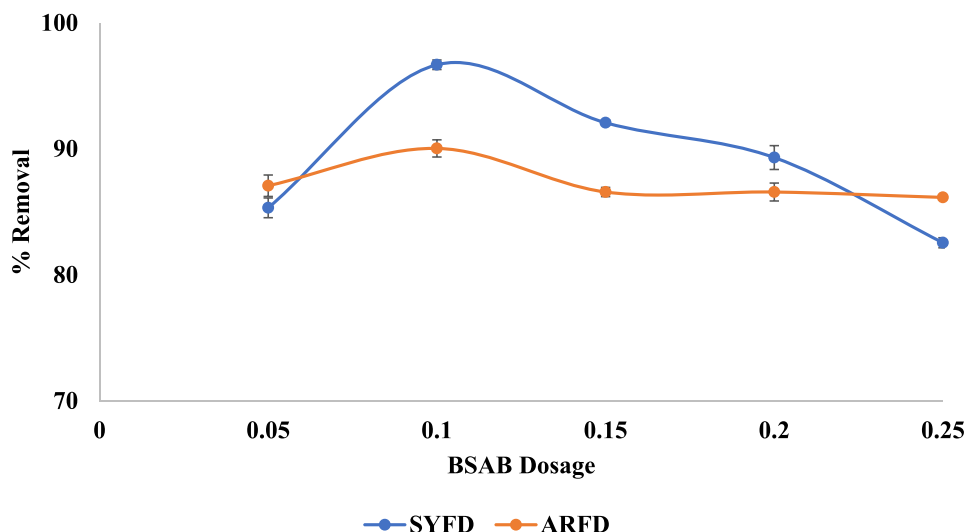**Fig. 1.** Effect of pH on ARFD and SYFD uptake onto BSAB.

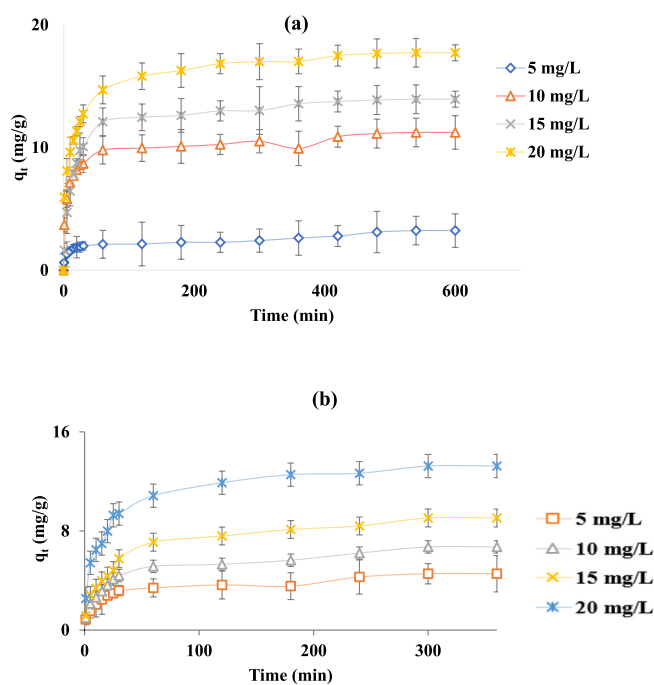Fig. 2. Effects of BSAB dosage for ARFD and SSYD adsorption.

Fig. 3. Impact of initial dye concentration and contact time on (a) ARFD and (b) SYFD adsorption.

is protonated in the acidic media while BSAB's surface is anionic beyond pH_{pzc}. This could lead to electrostatic attraction between BSAB and SYFD molecules. Also, SSY is an anionic dye molecule, with attached sulfonate groups, which can be electrostatically attracted to the cationic surface of BSAB. Hence, high removal efficiencies in the basic media. The removal efficiency was observed to decrease beyond pH 9 for both dyes. This can be as a result of the presence of excess negatively charged ions, jointly contributed by the adsorbent and the dyes leading to electrostatic repulsion (Alkahtani et al., 2017).

3.2.2. Influence of biochar dosage

The effect of BSAB dosage on ARFD and SYFD adsorption (Fig. 2) was investigated using a range of biosorbent doses ranging from 0.05 to 0.25 g per 100 mL dye solution. The dye sorption rate was found to increase as BSAB dosage increased. The increase in accessible sorption sites on the surface of BSAB explained these growing trends. At 0.1 g/100 mL adsorbent dosage, the maximal ARFD and SYFD removal efficiencies were reported to be 90.04 and 96.69 %, respectively. Further increase in the adsorbent dosage resulted in a steady decrease in the removal performance, which might be attributable to the agglomeration of BSAB particles in the presence of excess biochar in solution. This resulted to a decrease in the available sites for adsorption, as a result of which efficiency dropped (Pham et al., 2018).

3.2.3. Influence of contact time and initial concentration

Fig. 3a and b depicts the adsorbent-adsorbate interaction, as a function of initial concentration and time. A similar trend was observed for ARFD and SYFD uptake onto BSAB. An increase in initial concentration led to an increase in quantity of adsorbate adsorbed (mg/g). The adsorption of ARFD and SYFD onto BSAB was found to be very rapid in the first 60 min. As the contact time proceeds, the initial rapid adsorption rate gradually decreased until equilibrium was attained. The adsorption process was enhanced at higher initial concentrations, because a driving force that can overcome mass resistance transfer was provided (Abdullah Sani et al., 2023; Agbor Tabi et al., 2022).

3.3. Impact of temperature and thermodynamics studies

The effect of temperature and the thermodynamic studies on the removal of ARFD and SYFD onto BSAB was investigated at 26, 35, 45 and 55 °C as shown Fig. 4. A similar trend was observed for the both dyes. As the temperature was increased, the percentage removal decreased from 97.49 to 85.33 % and 95.12–86.18 % for ARFD and SYFD respectively. It can therefore be concluded that, lower temperatures favoured the adsorption processes. This could be due to the fact that an increase in temperature induces dissociation of the dyes from BSAB's surface as a result of intensifying kinetic energy (Chukwuemeka-Okorie et al., 2021).

The results of thermodynamic studies are presented in Table 3. ΔG^o values were negative (-7.62 to -2.62 kJ/mol and -7.38 to -4.99 kJ/mol) for ARFD and SYFD respectively, across all the studied temperatures. This established that the adsorption processes were feasible and spontaneous. The negative value of ΔH^o suggested that ARFD-BSAB and SYFD-BSAB adsorption systems were exothermic in nature while the negative value of ΔS^o specified a decreased randomness for each of the adsorption systems (Silva et al., 2021).
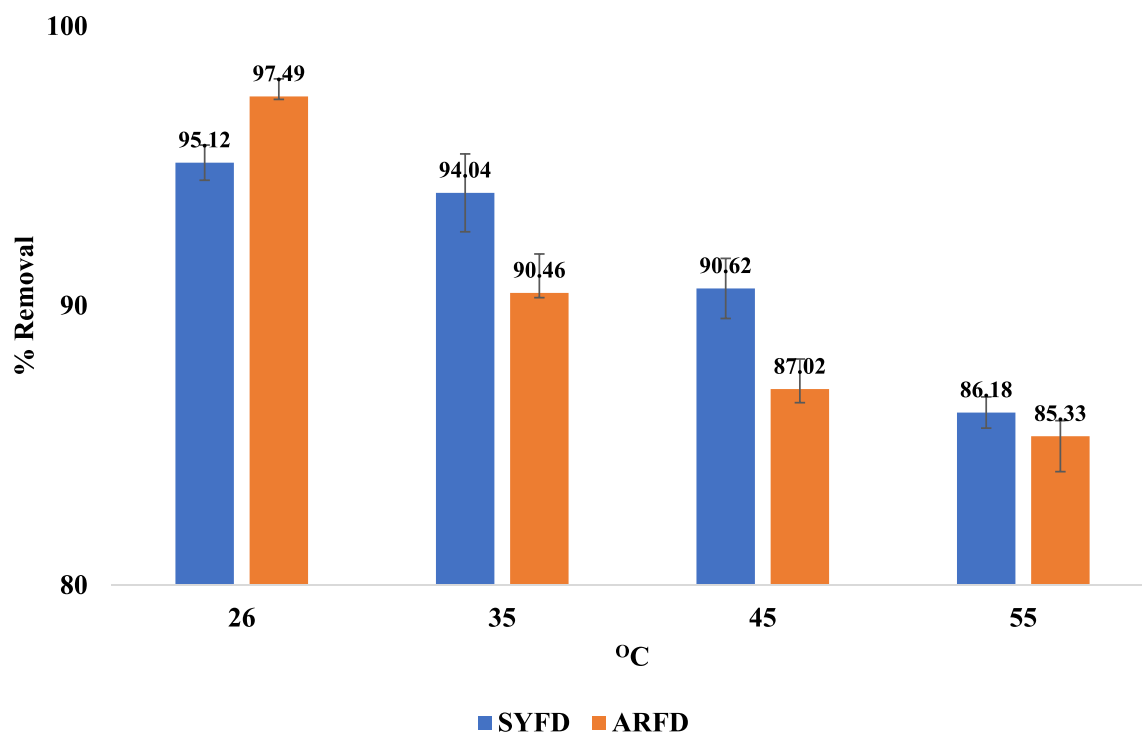
Fig. 4. Effect of temperature on ARFD and SYFD uptake onto BSAB.

Table 3
Thermodynamics study parameters of ARFD and SYFD onto BSAB.

Adsorbate	Temp. (K)	ΔS^o (JK^{-1} mol^{-1})	ΔG^o (kJ/mol)	ΔH^o (kJ/mol)
ARFD	299		−7.62	
	308	−178.22	−5.22	−60.47
	318		−3.11	
	328		−2.62	
SYFD	299		−7.38	
	308	−96.24	−7.07	−36.24
	318		−4.96	
	328		−4.99	

3.4. Kinetic studies

The kinetics of ARFD and SYFD adsorption onto BSAB were studied at various initial dye concentrations (5–20 mg/L) and described using the pseudo-first order, pseudo-second order, intraparticle diffusion, Elovich, and liquid film diffusion models. The experimental q_e values for the pseudo-first order kinetic model at 20 mg/L were 17.95 and 18.04 mg/g for ARFD and SYFD, respectively, while the calculated q_e values were 8.95 and 12.33 mg/g for the same dyes. Regardless of the fact that the R^2 values were reasonably high, ranging between 0.9328 and 0.9837 for ARFD as well as 0.9762 and 0.9861 for SYFD. However, the Average Relative error and Chi Square error values are higher than those of Pseudo second order. As a result, the adsorption process was not best characterised by the Pseudo-first order model. The experimental and calculated q_e values were quite close for the Pseudo-second order model, as evidenced by low error values and high R^2 values (Saloglu and Irmak, 2021), as shown in Table 4. These data suggest that the pseudo-second order kinetics model better explained the adsorption of ARFD and SYFD onto BSAB respectively. The pseudo-second order model has been understood as a type of Langmuir-kinetic model, whose adsorbate concentration and the overall number of binding sites are functions of the quantity of adsorbate adsorbed at equilibrium (Lopes et al., 2021).

The mass transfer phenomena of the adsorption processes were explained by the Intraparticle diffusion model. Because the linear plots did not pass through the origin, it can be concluded for both adsorption systems that intraparticle diffusion is not the rate-limiting step, as indicated by C_1 values of the first stage ranging from 1.5810 to 12.4220 for ARFD and 0.1005 to 0.3013 for SYFD. The constant C_1 was found to increase as the concentration of ARFD increased from 5 to 20 mg/L. This alteration in value is due to a rise in the thickness of the boundary layer, a decrease in the possibility of external mass transfer, and a significant increase in the amount of internal mass transfer. The high R^2 value confirms the model's suitability (Ghaedi et al., 2015). While the initial constant rate (α) is greater than the desorption coefficient (β) for ARFD and SYFD uptake onto BSAB, the Elovich model suggests that the adsorption process is dominated by chemisorption (Agbor Tabi et al., 2022). Considering the R^2 values of the Intraparticle diffusion and Liquid film diffusion models, it is possible to conclude that the adsorption process for both adsorption systems is regulated by internal and external diffusion at the stated conditions (Ojediran et al., 2021).

3.5. Isothermal studies

Mathematical isotherm modelling is a fundamental and significant part of adsorption investigations. Isotherm modelling is useful for observing the relationship between BSAB and the investigated food dyes at equilibrium. A thorough knowledge of this will greatly improve the design of the adsorption system, effluent treatment reactor, and BSAB-dye interaction pattern (Dada et al., 2021b; Katiyar et al., 2021; Reyna G et al., 2023). The initial concentration equilibrium data were analysed using the Langmuir, Freundlich, Dubinin-Radushkevich, and Redlich-Peterson mathematical isotherm models. Table 5 displays all mathematical isotherm models, their linear equations, and estimated parameters.

The Langmuir isotherm has been employed to explain adsorbate-adsorbent monolayer adsorption. The experimental data were fitted employing the Langmuir isotherm model, which yielded Q_m values of 15.17 and 33.27 mg/g, as well as R^2 values of 0.9156 and 0.8437 for ARFD and SYFD, respectively. RL is an important parameter of the Langmuir isotherm, the values obtained were less than one indicating

Table 4

Kinetic parameters for the adsorption of allura red and sunset yellow food dyes onto BSAB.

Kinetics	Linear equation		Initial ARFD concentration (mg/L)				Initial SYFD concentration (mg/L)			
			5	10	15	20	5	10	15	20
		$q_{e\ exp.}$	3.23	7.01	13.94	17.95	4.55	9.05	13.24	18.04
		Estimated parameters								
Pseudo first order	$log(q_e - q_t) = lnq_e - k_1 t$	$q_{e\ cal.}$	1.52	2.11	4.71	8.95	2.85	6.21	7.29	12.33
		K_1 (min)	0.003	0.006	0.006	0.006	0.013	0.013	0.014	0.015
		ARE	18.6969	38.8899	32.7484	36.0217	9.9361	7.6293	13.58	5.2726
		χ^2	1.9173	11.4415	18.1503	26.5286	1.0126	1.3005	4.8469	2.6403
		R^2	0.9328	0.9615	0.9837	0.9769	0.9837	0.9861	0.9815	0.9762
Pseudo second order	$\frac{t}{q_t} = \frac{1}{k_2 q_e^2} + \frac{t}{q_e}$	$q_{e\ cal.}$	2.53	7.04	14.22	17.99	4.5829	9.3721	13.5700	17.9338
		K_2 (min)	0.0400	0.0100	0.0200	0.0100	0.014	0.010	0.010	0.017
		ARE	1.2693	0.1731	0.0052	0.0895	0.1294	0.5976	0.4104	0.0943
		χ^2	0.0165	0.0007	0.00003	0.00005	0.0002	0.0112	0.0078	0.0006
		R^2	0.9937	0.9979	0.9994	0.9991	0.9885	0.9969	0.9990	0.9981
Elovich	$q_t = \frac{1}{\beta}ln(\alpha\beta) + \frac{1}{\beta}lnt$	α_{EI} (mg/g·min)	1.9437	7.8146	38.3562	353.61	2.0969	5.6504	11.9100	35.1423
		β_{EI} (g/mg)	2.5947	1.2825	0.5209	0.3186	1.5371	0.6863	0.5246	0.3924
		R^2	0.9842	0.9882	0.9888	0.9844	0.9839	0.9774	0.9856	0.9565
Intraparticle diffusion	$q_t = K_{Diff} t^{0.5} + C$	C_1 (mg/g)	1.5810	4.6170	8.9147	12.4420	0.3013	0.3970	0.1144	0.1005
		K_{Diff} (mg/g min$^{-1/2}$)	0.0536	0.1073	0.2268	0.2305	0.5583	0.9302	1.8487	1.9892
		R^2	0.9232	0.9209	0.8888	0.8386	0.9999	0.9764	0.9321	0.9875
Liquid film diffusion	$ln\left(1 - \left(\frac{q_t}{q_e}\right)\right) = -K_{LFD}t + C$	K_{LFD}	0.1026	0.1884	0.1374	0.1353	0.0092	0.0097	0.010	0.0170
		R^2	0.9188	0.9511	0.961	0.9386	0.9185	0.9585	0.9286	0.9554

Table 5

Evaluated isotherm parameters for the uptake of ARFD and SYFD onto BSAB.

Isotherm models	Linear equation	Evaluated parameters	ARFD	SYFD
Langmuir	$\frac{C_e}{q_e} = \frac{C_e}{q_{max}} + \frac{1}{q_{max}K_l}$	q_{max} (mg/g)	15.17	33.27
		R_L (L/mg)	0.0135–0.0626	0.0631–0.2519
		R^2	0.9156	0.8437
Freundlich	$logq_e = \frac{1}{n}logC_e + logK_f$	K_F (mg/g)	3.41	18.41
		$1/n$	0.5667	0.7513
		R^2	0.9696	0.9962
Redlich-Peterson	$ln\left(\frac{C_e}{q_e}\right) = BlnC_e - lnA$	B	0.2384	0.2824
		R^2	0.9754	0.5763
Dubinin-Radushkevich	$lnq_e = lnq_m - A_{DRK}\varepsilon^2$ $\varepsilon = RTln\left(1 + \frac{1}{C_e}\right)$ $E = -\left[\frac{1}{\sqrt{A_{D-R}}}\right]$	q_{DR} (mg/g)	12.66	24.07
		E (kJ/mol)	408.25	223.61
		R^2	0.9854	0.9706

Table 6

Comparison of adsorption efficiencies and ANN modelling of BSAB-ARFD and BSAB-SYFD with those presented in literature.

Food dyes	Adsorbent	Initial adsorbate concentration (mg/L)	q_{max} (mg/g)	ANN model	ANN architecture	Ref.
Allura red	Commercial activated carbon	300	72.85	x	x	(Alkahtani et al., 2017)
	Carob stones	–	94.88	x	x	(Erdoğan, 2019)
	Zirconia fibres	10	0.895	x	x	(Ávila-Martínez et al., 2020)
	Peanut hulls	–	51.66	x	x	(Torres-Perez et al., 2020)
	Bilghia sapida seed pods	5–20	15.17	✔	5-14-1	This study
Sunset yellow	Zinc oxide nanorods	5–40	83.33	✔	3-6-1	(Ghaedi et al., 2015)
	Alligator weed	100–300	132.00	x	x	(Kong et al., 2017)
	Chrysobolanus icaco shells	30–150	40.00	x	x	(Ekuma et al., 2019)
	Neodymium carbon	50–125	–	✔	3-6-1	(Ahmad et al., 2020)
	Coconut shells	–	0.327	x	x	(Ademoriyo and Enyoh, 2020)
	Groundnut shells	–	0.141	x	x	
	Bilghia sapida seed pods	5–20	33.27	✔	5-16-1	This study

favourable dye adsorption of the dyes onto BSAB. R^2 values of 0.9696 and 0.9962 for ARFD and SYFD in the Freundlich model were found to be greater than those in the Langmuir model. This is evidence of multilayer adsorption mechanisms (Inyinbor et al., 2023a). The Redlich-Peterson model, which combines the characteristics of the Langmuir and Freundlich models was investigated. Table 5 shows that the values of B tend to zero, indicating that the isotherms are approaching Freundlich form. However, because the R^2 value of the BSAB-SYFD was extremely low (05763), the R-P model was insufficient to explain this adsorption system.

In general, the Dubinin-Radushkevich isotherm was used to figure out the mechanism of the ARFD and SYFD dye onto BSAB with a Gaussian energy distribution onto a heterogeneous surface. The R^2 values were found to be 0.9854 and 0.9706, indicating that D-R model offered a good depiction of equilibrium data. The observation of a mean energy (E) value larger than 8 kJ/mol (408.25 and 223.61 kJ/mol) indicated chemisorption process (Ogunmodede et al., 2021).

Table 6 compares the adsorption capacity of BSAB-ARFD (15.15 mg/

Table 7

Statistical metrics for selecting hidden neurons for efficiency prediction of ARFD and SYFD onto BSAB.

Hidden neurons	ARFD		SYFD	
	MSE	R^2	MSE	R^2
1	40.11	0.917572	45.59	0.896241
2	23.03	0.92429	36.52	0.920832
3	18.29	0.949845	21.81	0.956288
4	16.02	0.956288	19.85	0.971604
5	22.37	0.95863681	19.53	0.963539
6	20.09	0.953748	17.29	0.969634
7	16.81	0.960204	14.18	0.966879
8	16.91	0.935863	14.81	0.961969
9	13.66	0.9516	13.01	0.972788
10	11.14	0.95668	12.79	0.974959
11	14.69	0.95942	14.81	0.969043
12	16.64	0.9516	16.02	0.968453
13	14.95	0.960008	13.29	0.978714
14	**9.96**	**0.977132**	14.53	0.976342
15	11.06	0.966486	11.96	0.976935
16	13.01	0.963931	**10.88**	**0.983469**
17	14.15	0.96452041	11.33	0.975749
18	11.36	0.967272	13.17	0.97259
19	17.46	0.937992	17.91	0.962165
20	19.27	0.945756	20.87	0.965306

Table 8

Results for varied activation functions for efficiency prediction.

Transfer function	ARFD	SYFD
Logsig	**0.944978**	invalid
Purelin	0.761605	0.758467
Tansig	0.933349	**0.97121**

g) and BSAB-SYFD (33.27 mg/g) with prior studies of allura red and sunset yellow dye removal reported in the literature. The adsorption capacities displayed in this study are substantially greater than the majority of the stated values. Also, the utilization of the ANN model for the development of architecture for predicting adsorption of efficiencies of ARFD and SYFD is scarce in literature.

3.6. Artificial Neural Network model findings

The performance of each of the hidden neurons is presented in Table 7. As shown, with reference to the minimum Mean Square Errors (MSE) 14 and 16 were considered the most appropriate number of hidden neurons in the hidden layer for ARFD and SYFD onto BSAB respectively. And hence, were chosen as the hidden neurons that suitably predicted the adsorption efficiency of BSAB for the two pollutants. The MSE obtained were 9.96 and 10.88 for ARFD and SYFD respectively.

For ANNs, there are always numerous neurons that work in correspondence of weights and bias, and the outputs can be generated from the inputs through these neurons. In the absence of activation functions, data are considered as linear, with the output of each layer being a linear function of the upper layer. As a result, no matter how many layers the ANN has, the outputs are a linear function of the inputs. The activation function determines whether a neuron is to be activated or not by calculating a weighted sum and then adding bias to it, which introduces non-linearity into the output of a neuron in order to obtain accurate outputs in ANNs. The neurons' weights and biases must be constantly updated based on the output error. This is made possible by the activation functions since the gradients are supplied together with the error to update the weights and biases (Feng and Lu, 2019). The variation of the *Purelin, Tansig and Logsig* activation functions (Table 8) used 14 and 16 numbers of hidden neurons for ARFD and SYFD respectively. The *Logsig* activation function provided the highest R^2 value of 0.944978 for ARFD. Whereas, the *Tansig* activation function gave an R^2 square value of 0.97121 for SYFD. Fig. 5a and b illustrated the regression plot for training, validation and testing of the experimental data for ARFD and SYFD respectively. This figure shows the overall of the prediction set, in the form of a network output against the experimental data efficiency. The architecture for the ANN model (5-14-1) for ARFD and (5-16-1) for SYFD uptake onto BSAB was then developed as depicted in Fig. 6a and b.

Fig. 7 (a–f) shows the comparison plot of predicted and experimental and predicted adsorption efficiency at different temperatures. Taking into account the variability of the experimental data that has successfully been captured by the optimal ANN conditions. A good agreement was observed between the predicted and the experimental data, which confirmed the efficiency of the ANN model. Similar findings have been
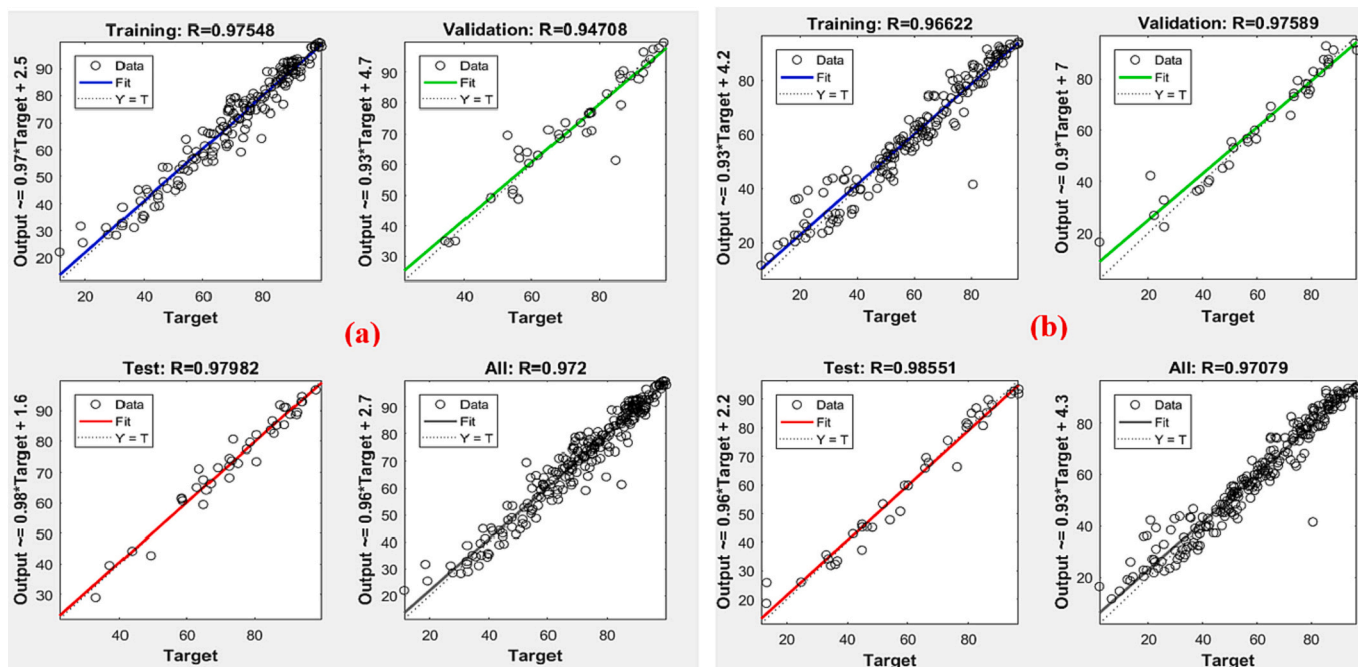

Fig. 5. Comparison of the experimental and predicted adsorption efficiency for (a) ARFD and (b) SYFD onto BSAB.
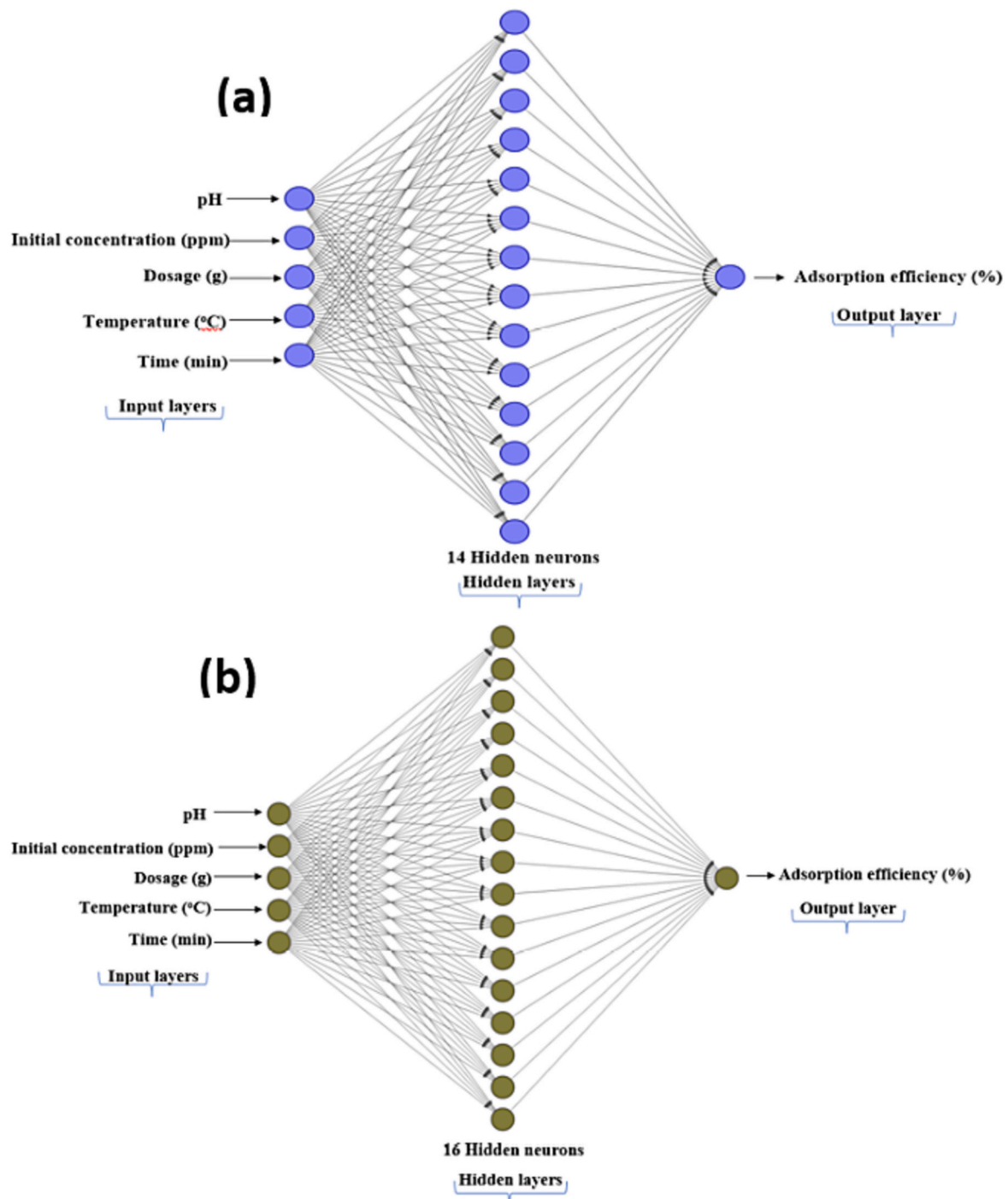
Fig. 6. A three- layered ANN model architecture for (a) ARFD and (b) SYFD.

reported (Karimi et al., 2019; Khan et al., 2016).

3.7. Desorption studies of the spent biochar

Fig. 8 depicted the desorption efficiencies of BSAB-ARFD and BSAB-SYFD adsorption systems. The desorption efficiency was obtained to be generally low. NaOH had the highest desorption efficiency (15.65 %) while NaCl, HCl and H_2O have a desorption efficiency of 7.51 %, 5.88 % and 5.38 % respectively, for ARFD. Also, for SYFD, the desorption efficiency was recorded in this order; NaOH > NaCl > HCl > H_2O (34.41 % > 7.06 % > 6.87 % > 6.82 %). This suggested that ALR and SYFD penetrated deep into BSAB's pores while some formed strong bond with

the biochar. Several contact points are present between adsorbent and adsorbates, which can establish adsorption energy. This can make the release of ARFD and SYFD from BSAB's surface tasking. This was supported by the values of desorption index (1.0188 and 1.3831) for ARFD and SYFD respectively (Dada et al., 2021a). These values indicated low degree of reversibility. *Bilghia sapida* waste is very abundant, which can make up for its commercial use as adsorbents (Mandal et al., 2020).

3.8. Possible mechanisms of interaction

The adsorption of ARFD and SYFD onto BSAB followed a similar trend. From the effect of pH on the adsorption systems, the proposed
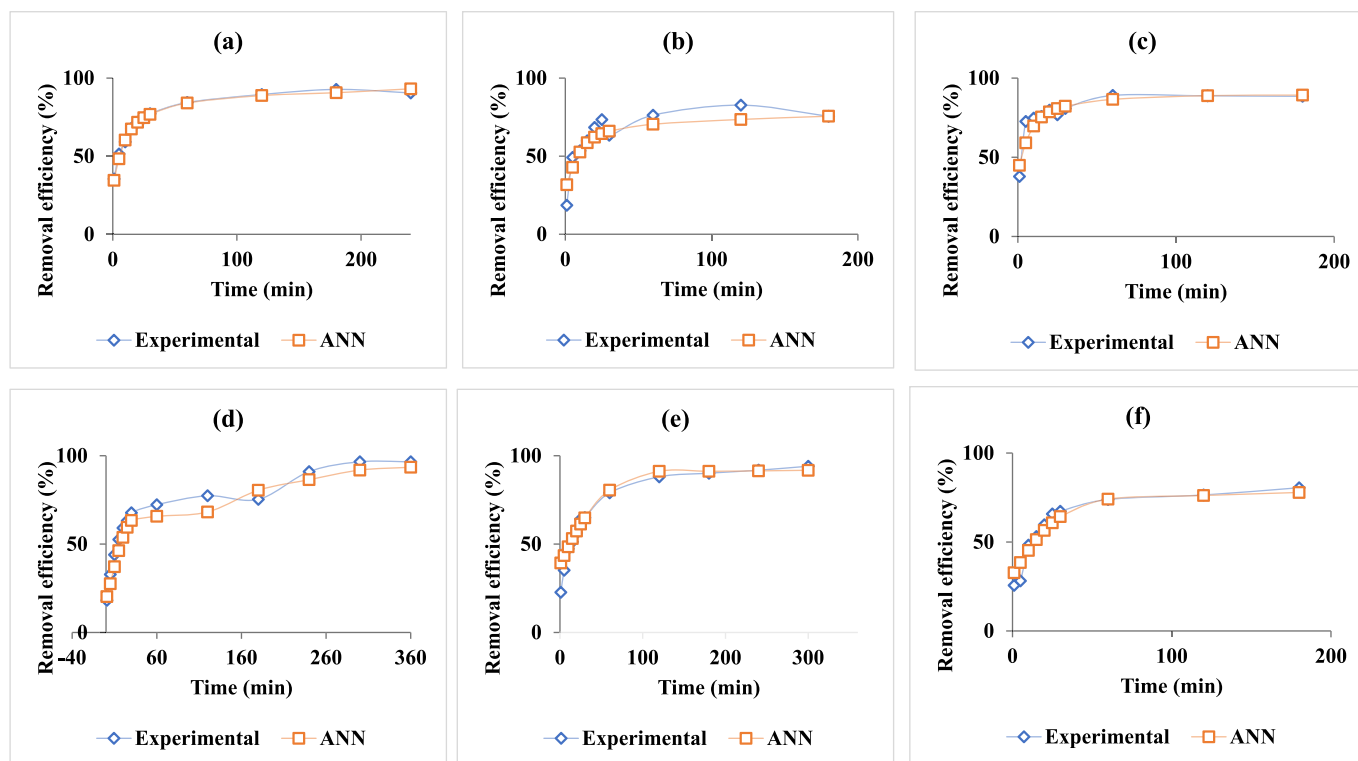
Fig. 7. ANN prediction of adsorption efficiency AT (a) 25 °C (b) 35 °C (c) 45 °C for ARFD, (d) 25 °C (e) 35 °C (f) 45 °C for SYFD.
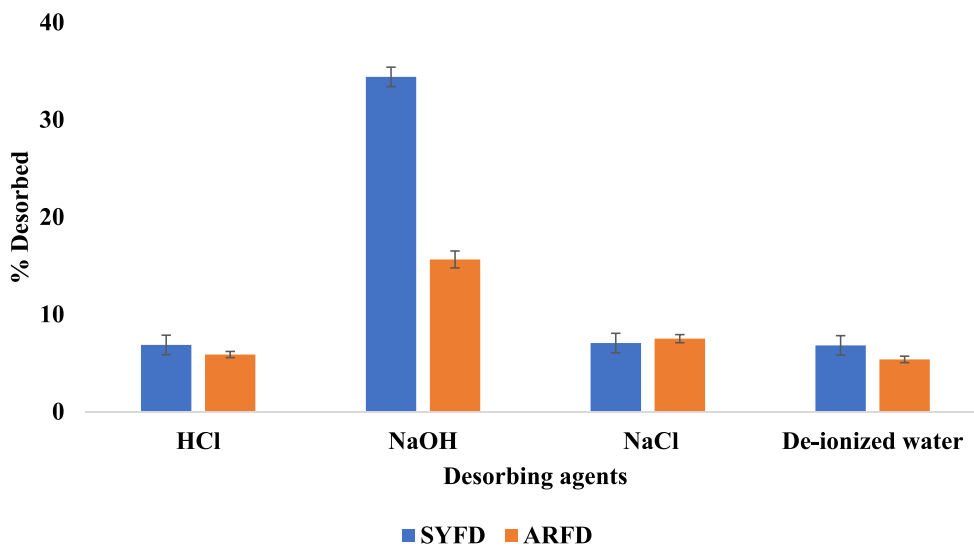

Fig. 8. Desorption efficiencies of BSAB for ARFD and SYFD removal.

mechanism of interaction is via electrostatic attraction. Similar findings have been reported (Agbor Tabi et al., 2022; Chukwuemeka-Okorie et al., 2021). The kinetic studies evaluation shows that both internal (intra-diffusion within pores) and external diffusion (surface functional groups interaction) controlled the adsorption systems. This claim was substantiated by the findings of the desorption studies. Low desorption efficiencies were obtained for both adsorption systems, possibly due to deep penetration of the dye molecules into BSAB pores or the formation of strong bonds between adsorbate and adsorbent (chemisorption) (da Costa et al., 2022).

3.9. Preparatory cost analysis

Examining the economic consequences of an adsorbent is necessary prior to large-scale implementation of adsorption techniques. The cost of the precursor, the activating agent, and the cost of operating the required appliances are some of the several factors that influence the net cost of activated carbon preparation (Ogunmodede et al., 2021; Ursue-guía et al., 2022). In addition, several processes such as sample collection, size reduction, carbonization and activation, neutralization, etc., are included in the cost analysis of an adsorbent. The feasibility of commercializing *Bilghia sapida* waste biochar (BSAB), developed from a readily available agricultural waste source was evaluated using a simple cost analysis. The analysis of the preparatory cost of 1 kg of BSAB in

contrast to commercially available activated carbon (CAC) is presented in Table S1. The production cost was much lower than the average market cost of CAC, hence the practicability of commercializing BSAB.

3.10. Future perspective

The current study explored the performance of BSAB for the uptake of ARFD and SYFD from aqueous media. The findings offered a promising outcome, hence, the possibilities of usage as an affordable means of wastewater remediation in confectionery industries. The desorption studies which offered insight into the reusability potential of spent adsorbents and solutions to the issue of proper disposal was also investigated. In addition, efficiency validation using ANN was also evaluated on BSAB-ARFD and BSAB-SYFD adsorption systems. However, real industrial effluents contain several components that could have synergistic or antagonist impacts on an adsorption process. The adsorption of multicomponent effluent as well as column studies should be considered for future studies, utilizing the findings of the current study. Also, the performance of BSAB on the removal of the investigated dye could not be regarded as a standard for its efficiency on other water contaminants. It is therefore recommended that BSAB be tested for the removal of other water contaminants such as pharmaceuticals, heavy metals and other Endocrine Disrupting Chemicals (EDCs).

4. Conclusions

The highly effective removal of Allura red (ARFD) and Sunset yellow (SYFD) food colours from an aqueous solution was achieved by employing acid-activated *Bilghia sapida* wastes (BSAB) as an environmentally friendly adsorbent. SEM coupled with EDX and FTIR spectroscopy, were used to characterize BSAB. ARFD and SYFD had maximal adsorption capacities of 15.17 and 33.27 mg/g respectively at concentrations of 20 mg/L. Both the Freundlich isotherm model and the pseudo-second order kinetic model better described the adsorption data for both adsorption systems. According to the findings of the Gibbs free energy and enthalpy changes, adsorption of ARFD and SYFD was spontaneous and exothermic. ARFD and SYFD adsorption was governed by both intraparticle diffusion and liquid film diffusion. All of the desorbing agents studied had low efficiency in the desorption trials. The desorption index values of 1.0188 and 1.3831 obtained for ARFD and SYFD, respectively, supported this, showing a low degree of reversibility. The optimum transfer function, MSE, and R^2 values for ARFD were (Logsig, 9.96, 0.9771) and (Tansig, 10.88, 0.9835) for SYFD, as predicted by the ANN model. The ANN architecture of 5-14-1 and 5-16-1 was successfully designed for ARFD and SYFD adsorption systems. BSAB have a high potential for food colour removal from confectionery industrial wastewaters.

Supplementary data to this article can be found online at https://doi.org/10.1016/j.biteb.2023.101709.

CRediT authorship contribution statement

Bankole Deborah: Methodology, Original draft, Writing, review & editing. **Inyinbor Adejumoke:** Conceptualization, Methodology & Supervision **Oluyori Abimbola:** Conceptualization, Methodology & Supervision. **Arowolo Micheal:** Software & Editing.

Declaration of competing interest

The authors declare that there are no known competing personal relationships or financial interests that could have influenced the work reported in this paper.

Data availability

Data will be made available on request.

References

Abdullah Sani, N.S., Ang, W.L., Mohammad, A.W., Nouri, A., Mahmoudi, E., 2023. Sustainable synthesis of graphene sand composite from waste cooking oil for dye removal. Sci. Rep. 13 https://doi.org/10.1038/s41598-023-27477-8.

Ademoriyo, C., Enyoh, C., 2020. Batch adsorption studies of sunset yellow and tartrazine using coconut and groundnut shells. J. Biomed. Res. Environ. Sci. 1, 163–172. https://doi.org/10.37871/jbres1138.

Agbor Tabi, G., Ngouateu Rene Blaise, L., Daouda, K., Naphtali Odogu, A., Aime Victoire, A., Nsami Julius, N., Joseph Mbadcam, K., 2022. Non-linear modelling of the adsorption of Indigo Carmine dye from wastewater onto characterized activated carbon/volcanic ash composite. Arab. J. Chem. 15, 103515 https://doi.org/10.1016/j.arabjc.2021.103515.

Ahmad, Z.U., Yao, L., Lian, Q., Islam, F., Zappi, M.E., Gang, D.D., 2020. The use of artificial neural network (ANN) for modeling adsorption of sunset yellow onto neodymium modified ordered mesoporous carbon. Chemosphere 256. https://doi.org/10.1016/j.chemosphere.2020.127081.

Ahmad, M.A., Afandi, N.S., Adegoke, K.A., Bello, O.S., 2016. Optimization and batch studies on adsorption of malachite green dye using rambutan seed activated carbon. Desalin. Water Treat. 57, 21487–21511. https://doi.org/10.1080/19443994.2015.1119744.

Al Shamari, Y.M.G., Alwarthan, A.A., Wabaidur, S.M., Khan, M.A., Alqadami, A.A., Siddiqui, M.R., 2020. New ultra performance liquid chromatography-mass spectrometric method for the determination of allura red in soft drinks using corncob as solid phase extraction sorbent: analysis and food waste management approach. J. King Saud Univ. Sci. 32, 1135–1141. https://doi.org/10.1016/j.jksus.2019.10.011.

Alkahtani, S.A., Abu-Alrub, S.S., Mahmoud, A.M., 2017. Adsorption of food coloring Allura Red dye (E129) from aqueous solutions using activated carbon. Int. J. Food Allied Sci. 3, 10. https://doi.org/10.21620/ijfaas.2017110-26.

Ávila-Martínez, A.K., Roque-Ruiz, J.H., Torres-Pérez, J., Medellín-Castillo, N.A., Reyes-López, S.Y., 2020. Allura Red dye sorption onto electrospun zirconia nanofibers. Environ. Technol. Innov. 18 https://doi.org/10.1016/j.eti.2020.100760.

Bashir, M., Mohan, C., Tyagi, S., Annachhatre, A., 2022. Copper removal from aqueous solution using chemical precipitation and adsorption by Himalayan pine forest residue as biochar. Water Sci. Technol. 86, 530–554. https://doi.org/10.2166/wst.2022.222.

Chukwuemeka-Okorie, H.O., Ekuma, F.K., Akpomie, K.G., Nnaji, J.C., Okereafor, A.G., 2021. Adsorption of tartrazine and sunset yellow anionic dyes onto activated carbon derived from cassava sievate biomass. Appl Water Sci 11, 1–8. https://doi.org/10.1007/s13201-021-01357-w.

da Costa, T.B., da Silva, T.L., Costa, C.S.D., da Silva, M.G.C., Vieira, M.G.A., 2022. Chromium adsorption using Sargassum filipendula algae waste from alginate extraction: batch and fixed-bed column studies. Chem. Eng. J. Adv. 11 https://doi.org/10.1016/j.ceja.2022.100341.

da Silva Alves, D.C., Healy, B., Pinto, L.A.d.A., Cadaval, T.R.S., Breslin, C.B., 2021. Recent developments in Chitosan-based adsorbents for the removal of pollutants from aqueous environments. Molecules 26. https://doi.org/10.3390/molecules26030594.

Dada, A.O., Adekola, F.A., Odebunmi, E.O., Ogunlaja, A.S., Bello, O.S., 2021a. Two–three parameters isotherm modeling, kinetics with statistical validity, desorption and thermodynamic studies of adsorption of Cu(II) ions onto zerovalent iron nanoparticles. Sci. Rep. 11, 1–15. https://doi.org/10.1038/s41598-021-95090-8.

Dada, A.O., Inyinbor, A.A., Bello, O.S., Tokula, B.E., 2021b. Novel plantain peel activated carbon–supported zinc oxide nanocomposites (PPAC-ZnO-NC) for adsorption of chloroquine synthetic pharmaceutical used for COVID-19 treatment. Biomass Convers. Biorefin. https://doi.org/10.1007/s13399-021-01828-9.

Darryle, C.M., Acayanka, E., Takam, B., Line, L.N., Kamgang, G.Y., Laminsi, S., Sellaoui, L., Bonilla-Petriciolet, A., 2021. Influence of plasma-based surface functionalization of palm fibers on the adsorption of diclofenac from water: experiments, thermodynamics and removal mechanism. J. Water Process Eng. 43 https://doi.org/10.1016/j.jwpe.2021.102254.

Ekuma, F.K., Chukwuemeka-Okorie, H.O., Okoyeagu, A., Chimeziri, C.C., 2019. Studies on the adsorption of tartrazine and sunset yellow dyes from aqueous solution using activated gbafilo (Chrysobalanus icaco) shell. J. Chem Soc. Niger. 44, 937–947.

Erdoğan, F.O., 2019. Comparison of activated carbon produced from carob stones with 4a zeolite for Allura Red Ac dye. J. Sci. Technol. 9, 75–79.

Feng, J., Lu, S., 2019. Performance analysis of various activation functions in artificial neural networks. J. Phys. Conf. Ser. 1237 https://doi.org/10.1088/1742-6596/1237/2/022030.

Fu, X.G., Shi, K., Xue, J.L., Chen, C., Bai, Y., Qiao, Y.L., Liu, Y.X., Hu, X.M., Gao, Y., Yu, H., 2021. Systematic adsorption process of petroleum hydrocarbon by immobilised petroleum-degradation bacteria system in degradation pathways. Pet. Sci. 18, 1543–1550. https://doi.org/10.1016/j.petsci.2021.09.009.

Ghaedi, M., Zeinali, N., Maghsoudi, M., Purkait, M.K., 2015. Artificial Neural Network (ANN) method for modeling of sunset yellow dye adsorption using nickel sulfide nanoparticle loaded on activated carbon: kinetic and isotherm study. J. Dispers. Sci. Technol. 36, 1339–1348. https://doi.org/10.1080/01932691.2014.964359.

Gičević, A., Hindija, L., Karačić, A., 2020. Toxicity of azo dyes in pharmaceutical industry. IFMBE Proc. 73, 581–587. https://doi.org/10.1007/978-3-030-17971-7_88.

Hosseinian-Roudsari, A., Shahidi, S.A., Ghorbani-HasanSaraei, A., Hosseini, S., Fazeli, F., 2022. A new electroanalytical approach for sunset yellow monitoring in fruit juices based on a modified sensor amplified with nano-catalyst and ionic liquid. Food Chem. Toxicol. 168 https://doi.org/10.1016/j.fct.2022.113362.

Inyinbor, A.A., Bankole, D.T., Adekola, F.A., Bello, O.S., Oreofe, T., Amone, K., Lukman, A.F., 2023a. Chemometrics validation of adsorption process economy: case study of acetaminophen removal onto quail eggshell adsorbents. Sci. African 19. https://doi.org/10.1016/j.sciaf.2022.e01471.

Inyinbor, A.A., Bankole, D.T., Solomon, P., 2023b. Adsorptive removal of acetaminophen onto acid-modified *Raphia hookeri* fruit epicarp. Biomass Convers. Biorefin. https://doi.org/10.1007/s13399-023-03871-0.

Karimi, R., Yousefi, F., Ghaedi, M., Rezaee, Z., 2019. Comparison the behavior of ZnO–NP–AC and Na, K doped ZnO–NP–AC for simultaneous removal of Crystal Violet and Quinoline Yellow dyes: modeling and optimization. Polyhedron 170, 60–69. https://doi.org/10.1016/j.poly.2019.05.038.

Katiyar, R., Patel, A.K., Nguyen, T.B., Singhania, R.R., Chen, C.W., Di Dong, C., 2021. Adsorption of copper (II) in aqueous solution using biochars derived from Ascophyllum nodosum seaweed. Bioresour. Technol. 328, 124829 https://doi.org/10.1016/j.biortech.2021.124829.

Khan, T., Isa, M.H., Ul Mustafa, M.R., Yeek-Chia, H., Baloo, L., Binti Abd Manan, T.S., Saeed, M.O., 2016. Cr(VI) adsorption from aqueous solution by an agricultural waste based carbon. RSC Adv. 6, 56365–56374. https://doi.org/10.1039/c6ra05618k.

Kong, Q., Liu, Q., Miao, M.S., Liu, Y.Z., Chen, Q.F., Zhao, C.S., 2017. Kinetic and equilibrium studies of the biosorption of sunset yellow dye by alligator weed activated carbon. Desalin. Water Treat. 66, 281–290. https://doi.org/10.5004/dwt.2017.20223.

Lopes, G.K.P., Zanella, H.G., Spessato, L., Ronix, A., Viero, P., Fonseca, J.M., Yokoyama, J.T.C., Cazetta, A.L., Almeida, V.C., 2021. Steam-activated carbon from malt bagasse: optimization of preparation conditions and adsorption studies of sunset yellow food dye. Arab. J. Chem. 14 https://doi.org/10.1016/j.arabjc.2021.103001.

Mandal, A., Bar, N., Das, S.K., 2020. Phenol removal from wastewater using low-cost natural bioadsorbent neem (Azadirachta indica) leaves: adsorption study and MLR modeling. Sustain. Chem. Pharm. 17, 100308 https://doi.org/10.1016/j.scp.2020.100308.

Moradi, O., Sharma, G., 2021. Emerging novel polymeric adsorbents for removing dyes from wastewater: a comprehensive review and comparison with other adsorbents. Environ. Res. 201 https://doi.org/10.1016/j.envres.2021.111534.

Obayomi, K.S., Lau, S.Y., Zahir, A., Meunier, L., Jianhua, Z., Dada, A.O., Rahman, M.M., 2023. Removing methylene blue from water: a study of sorption effectiveness onto nanoparticles-doped activated carbon. Chemosphere 313. https://doi.org/10.1016/j.chemosphere.2022.137533.

Ogunmodede, J., Akanji, S.B., Bello, O.S., 2021. Moringa oleifera seed pod-based adsorbent for the removal of paracetamol from aqueous solution: a novel approach toward diversification. Environ. Prog. Sustain. Energy 40, 1–11. https://doi.org/10.1002/ep.13615.

Ojediran, J.O., Dada, A.O., Aniyi, S.O., David, R.O., Adewumi, A.D., 2021. Mechanism and isotherm modeling of effective adsorption of malachite green as endocrine disruptive dye using Acid Functionalized Maize Cob (AFMC). Sci. Rep. 11, 1–15. https://doi.org/10.1038/s41598-021-00993-1.

Oladipo, A.C., Abodunrin, T.O., Bankole, D.T., Oladeji, O.S., Egharevba, G.O., Bello, O.S., 2021. Environmental applications of metal-organic frameworks and derivatives: recent advances and challenges. ACS Symp. Ser. 257–298. https://doi.org/10.1021/bk-2021-1394.ch011.

Pham, Tien Duc, Bui, T.T., Nguyen, V.T., Van Bui, T.K., Tran, T.T., Phan, Q.C., Pham, Tien Dat, Hoang, T.H., 2018. Adsorption of polyelectrolyte onto nanosilica synthesized from rice husk: characteristics, mechanisms, and application for antibiotic removal. Polymers (Basel) 10. https://doi.org/10.3390/polym10020220.

Reyna G, S.D., Yedidia, V.P., María del Rosario, M.M., Jaime, L.C., Dalia, I.S.M., Ma. A, C.M., 2023. Behavior of the adsorption of Allura Red dye by chitosan beads and nanoparticles. Nanotechnol. Environ. Eng. 8, 49–62. https://doi.org/10.1007/s41204-022-00268-8.

Reynel-Ávila, H.E., Aguayo-Villarreal, I.A., Diaz-Muñoz, L.L., Moreno-Pérez, J., Sánchez-Ruiz, F.J., Rojas-Mayorga, C.K., Mendoza-Castillo, D.I., Bonilla-Petriciolet, A., 2022. A review of the modeling of adsorption of organic and inorganic pollutants from water using artificial neural networks. Adsorpt. Sci. Technol. 2022 https://doi.org/10.1155/2022/9384871.

Saha, T.K., Bishwas, R.K., Karmaker, S., Islam, Z., 2020. Adsorption characteristics of Allura Red AC onto sawdust and hexadecylpyridinium bromide-treated sawdust in aqueous solution. ACS Omega 5, 13358–13374. https://doi.org/10.1021/acsomega.0c01493.

Saloglu, D., Irmak, O., 2021. Removal of azo dyes – tartrazine , carmoisine , and Allura Red – from wastewater using Spirulina biomass-immobilized alginate beads : equilibrium , kinetics , thermodynamics , desorption , and reusability, 220, 431–445. https://doi.org/10.5004/dwt.2021.27010.

Silva, M.C., Spessato, L., Silva, T.L., Lopes, G.K.P., Zanella, H.G., Yokoyama, J.T.C., Cazetta, A.L., Almeida, V.C., 2021. H3PO4–activated carbon fibers of high surface area from banana tree pseudo-stem fibers: adsorption studies of methylene blue dye in batch and fixed bed systems. J. Mol. Liq. 324 https://doi.org/10.1016/j.molliq.2020.114771.

Šuleková, M., Smrčová, M., Hudák, A., Heželová, M., Fedorová, M., 2017. Organic colouring agents in the pharmaceutical industry. Folia Vet. 61, 32–46. https://doi.org/10.1515/fv-2017-0025.

Temitope Bankole, D., Peter Oluyori, A., Abosede Inyinbor, A., 2022. Potent adsorbent prepared from Bilghia sapida waste material: Surface chemistry and morphological characterization. Mater. Today Proc. 65, 3665–3670. https://doi.org/10.1016/j.matpr.2022.06.238.

Tokula, B.E., Dada, A.O., Inyinbor, A.A., Obayomi, K.S., Bello, O.S., Pal, U., 2023. Agro-waste based adsorbents as sustainable materials for effective adsorption of Bisphenol A from the environment: a review. J. Clean. Prod. 388 https://doi.org/10.1016/j.jclepro.2022.135819.

Torres-Perez, J., Huang, Y., Bazargan, A., Khoshand, A., McKay, G., 2020. Two-stage optimization of Allura direct red dye removal by treated peanut hull waste. SN Appl. Sci. 2, 1–12. https://doi.org/10.1007/s42452-020-2196-3.

Ursueguía, D., Díaz, E., Ordóñez, S., 2022. Adsorbents selection for the enrichment of low-grade methane coal mine emissions by temperature and pressure swing adsorption technologies. J. Nat. Gas Sci. Eng. 105 https://doi.org/10.1016/j.jngse.2022.104721.

Wang, J., Wang, S., 2019. Preparation, modification and environmental application of biochar: a review. J. Clean. Prod. 227, 1002–1022. https://doi.org/10.1016/j.jclepro.2019.04.282.